Astron. Astrophys. 318, 729–740 (1997)

ASTRONOMY
AND
ASTROPHYSICS

Studies of the association of faint blue and luminous galaxies using the Hitchhiker parallel camera

J.B. Jones[1], **S.P. Driver**[2], **S. Phillipps**[3], **J.I. Davies**[1], **I. Morgan**[1], **and M.J. Disney**[1]

[1] Department of Physics and Astronomy, University of Wales College of Cardiff, P.O. Box 913, Cardiff, CF2 3YB, Wales, UK (jbj@astro.cf.ac.uk)
[2] School of Physics, University of New South Wales, Sydney, NSW 2052, Australia
[3] Astrophysics Group, Department of Physics, University of Bristol, Tyndall Avenue, Bristol, BS8 1TL, England, UK

Received 12 September 1995 / Accepted 11 June 1996

Abstract. At B magnitudes $\gtrsim 24$ there is a well-known excess of galaxies (compared to standard models) which is probably due to an (evolving) population of sub-L^* galaxies at moderate redshifts ($\lesssim 0.4$). One particular hypothesis which is hard to test directly via number counts or even redshift surveys is the possibility that the faint blue galaxies are in fact sub-galactic objects destined to merge by the present day to form current giant galaxies. If this were the case we might expect to find the faint blue galaxies in the vicinity of $\simeq L^*$ galaxies (at redshifts $\simeq 0.2$ to 0.4) with which they can merge (the blue galaxies are already known to be weakly clustered among themselves, limiting the possibility for multiple mergers of small fragments).

In the present paper we look for evidence of such clustering of faint blue galaxies around larger systems using candidates chosen photometrically from deep multicolour CCD images using the Hitchhiker parallel CCD camera. A sample of candidate L^* galaxies expected to lie at redshifts $z \simeq 0.2$ to 0.4 has been selected on the basis of apparent magnitude (B = $20\overset{\mathrm{m}}{.}5$ to $22\overset{\mathrm{m}}{.}0$) and colours typical of early-type spirals. The distribution of 152 blue galaxies having $23\overset{\mathrm{m}}{.}5 < \mathrm{B} < 25\overset{\mathrm{m}}{.}0$, $(\mathrm{B}-\mathrm{R})_{\mathrm{c}} < 1\overset{\mathrm{m}}{.}2$, around 13 candidate L^* galaxies has been determined. No evidence has been found for any preferential clustering of blue galaxies about the L^* candidates; the observed overdensity within 60 arcsec of the L^* candidates is -0.02 ± 0.76 per candidate. We have also looked for clustering between other photometrically selected samples (such as faint blue and faint red objects). Null results have been found in all cases, placing significant limits on the scenarios wherein dwarfs at medium redshifts are removed via mergers with larger objects.

Key words: galaxies: interactions – galaxies: evolution – galaxies: photometry – galaxies: statistics – cosmology: observations

Send offprint requests to: J.B. Jones

1. Introduction

Deep imaging surveys have revealed a large population of blue galaxies at faint magnitudes (e.g. Tyson 1988; Lilly et al. 1991; Metcalfe et al. 1991, 1995; Driver et al. 1994a), which becomes increasingly important at fainter limits. The exact nature of these objects remains uncertain; for instance it is not clear whether these blue galaxies themselves have more extreme properties at fainter magnitudes, or whether their relative numbers increase. Spectroscopic surveys suggest that they are found predominantly at moderate redshifts ($z \simeq 0.1$ to 0.6) (e.g. Colless et al. 1990, 1993; Cowie et al. 1991; Lilly et al. 1991; Glazebrook et al. 1995a) and that they tend to have strong [OII] emission (Koo et al. 1995). Since they are not predicted by standard galaxy models, these blue galaxies have often been cited as the strongest evidence for galaxy evolution with redshift (Broadhurst et al. 1988; Broadhurst et al. 1992).

Any convincing explanation of their nature must account for the absence of any clear local counterpart to the faint blue galaxies. One possible model envisages that these objects have faded over time, implying luminosity evolution of either the entire galaxy population (e.g. Lilly et al. 1991) or of a subset of it (Broadhurst et al. 1988; Phillipps & Driver 1995; Driver et al. 1995a). Alternatively, the blue galaxies may have experienced density evolution. Merging (Rocca-Volmerange & Guiderdoni 1990; Broadhurst et al. 1992; Carlberg 1992) of the faint galaxies, either with each other or with more luminous objects, provides a mechanism for reducing their numbers by the present time (Koo 1990; Carlberg & Charlot 1992).

Giraud (1992) performed high resolution imaging of samples of blue galaxies, identifying three distinct morphological classes. More recently, Colless et al. (1994) have studied the light profiles of a sample of faint blue galaxies from the Colless et al. (1990, 1993) redshift survey using images taken in excellent seeing with the Canada-France-Hawaii Telescope. They found that faint galaxies exhibiting [OII] line emission often have nearby companions, suggesting interactions are important in activating star formation.

Recent HST results show a large fraction (around a half) of faint galaxies to have irregular or peculiar morphology (e.g. Casertano et al. 1995; Driver et al. 1995a,b). Of these maybe one third (i.e. $\sim 15\%$ of the total population) appear to be interacting (e.g. Driver et al. 1995b; Glazebrook et al. 1995b). This clearly suggests a role for interactions or mergers in the evolution of the faint blue galaxy population. Furthermore, Burkey et al. (1994) found that $\sim 34\%$ of HST galaxies at redshifts 0.4 to 0.7 had close companions compared to $\sim 7\%$ locally, suggesting that $\sim 13\%$ of the distant population may have disappeared by merging. However, Woods et al. (1995) using a similar technique find no excess pairs in the deep data.

Various different merging models have been advocated. The faint blue galaxies may gradually merge with one another to form more massive objects, or may be accreted into massive dark haloes (Rocca-Volmerange & Guiderdoni 1990). Cowie et al. (1991) suggested that the faint galaxies have 'parent' giant galaxies with which they have since merged, implying a physical (clustering) association between the two (see also Cowie et al. 1995). Kauffmann et al. (1994) have fitted faint number counts using detailed models of hierarchical galaxy formation (in a cold dark matter context) in which satellite galaxy haloes merge with more massive dark haloes of giant galaxies. On the other hand, Dalcanton (1993) has argued that the conservation of luminosity during mergers of the blue galaxies would lead to an excess integrated luminosity over that observed. The observed thinness of the discs of spiral galaxies may also constrain the importance of mergers in the evolution of these objects (e.g. Tóth & Ostriker 1992). The general level of clustering among faint blue galaxies appears to be low (Efstathiou et al. 1991; Pritchet & Infante 1992; see also Neuschaefer & Windhorst 1995) which may constrain direct merger models. On the other hand, Cole et al. (1994) find that dwarfs and giants at moderate redshifts occupy the same general structures and have very similar large-scale clustering properties.

A model of mergers of dwarfs with giants might therefore be tested by measuring the small-scale clustering of faint blue galaxies around a sample of candidate giant galaxies; this is the approach we adopt here (see Jones et al. 1994). A preferential clustering of the faint blue galaxies around giants would imply that they are dwarfs at similar redshifts to the giants and might favour merging models over fading in accounting for the lack of these low luminosity systems in the nearby Universe. Conversely, the absence of any excess around giants might be interpreted as evidence against the merging of dwarfs with more luminous parents (see also Bernstein et al. 1994). Using data from the Hitchhiker camera, we study the numbers of these objects around photometrically selected candidate giants and compare them with a random distribution in order to search for an excess consistent with the blue galaxies being dwarfs associated with parent giants.

In Sects. 2 and 3 we describe the observational data and the data reduction methods. In Sect. 4 the image detection process is detailed together with the techniques used for aperture photometry. The definition of samples of faint blue galaxies and candidate luminous galaxies are discussed in Sect. 5, and the association of the blue galaxies with the giants is determined. We model the distribution of random samples of faint images to account for the effects of the limited areas of data frames and to demonstrate that the light of bright images does not mask faint images to affect significantly the statistics of fainter objects. Sect. 6 considers the association between other photometrically selected samples. Sect. 7 presents a detailed investigation of the errors in the analysis. Finally, the implications of the results for the evolutionary history of the galaxy population are briefly considered.

2. Hitchhiker camera observations

The data consist of deep B- and R-band images of four fields obtained with the Hitchhiker parallel CCD camera on the 4.2m William Herschel Telescope on La Palma. The camera, described in Driver (1994), performs imaging in an off-axis field, 7 arcmin from the optical axis, while the telescope is used for its normal spectroscopic programmes. Using a dichroic beam splitter, data are recorded from the same field in two colours simultaneously.

The data used here were collected over several observing periods in 1991 and in 1993. They are summarised in Table 1. Example R band data are presented in Fig. 1, where the candidate L^* and faint blue galaxies of Sect. 5.1 are marked. The 1991 data are described in detail by Driver (1994) (and one field by Driver et al. 1994a). Total integration times on the fields ranged between 32 and 125 minutes through each filter. Individual exposures were typically of 5–10 minutes duration. The fields used were all at moderate or high galactic latitude. Seeing was around 1.5 arcsec (full-width at half-maximum) in the R band; image size measurements made with the KAPPA software package, supplied by the Starlink project, are presented in Table 1. Reduced frames were all about $5' \times 3'$ in extent; this means that clustering on scales up to $\sim 1\,\mathrm{Mpc}$ can be investigated at the distances at which we expect to see L^* galaxies. Note that if merging takes a few (say 5) dynamical times, only neighbours within $\sim \frac{1}{3}\,\mathrm{Mpc}$ of a galaxy with rotation/dispersion velocity $\sim 300\,\mathrm{kms}^{-1}$ could be expected to merge in the $\sim 5\,\mathrm{Gyr}$ since $z \sim 0.4$. Typically 200–300 galaxies are detected in each field.

3. Data reduction

The parallel mode of operation of the Hitchhiker camera, without any control of the pointing of the telescope, requires that the data be reduced in a slightly non-standard manner. These methods are described in full by Driver (1994) and summarised by Driver et al. (1994a). Firstly, bias signal subtraction was performed by removing a mean bias level calculated from the CCD bias strips of each raw data frame. The validity of this approach has been verified by testing the intensity of the bias signal across the whole frame; no significant structure has been found. The data frames suffer from an essentially circularly-symmetric vignetting pattern (caused by instrumental optical components). Because this varies with the focussing of the camera lenses, and because it is not always possible to obtain nightly flatfielding

Table 1. Observational data

R.A. (1950.0)	Dec. (1950.0)	Date	Integration time (min.)		R band seeing (FWHM)	Area of reduced data frame
			B band	R band		
$12^h\,29.5^m$	$+26^o\,26'$	1991 Feb 15	120	120	1.6 arcsec	$5.5' \times 3.0'$
11 40.1	+19 49	1991 Feb 12	75	75	1.3	5.5×3.0
13 37.8	+11 28	1993 Feb 28, Mar 2	40	60	1.6	5.0×3.3
15 47.6	+21 35	1993 May 22	32	32	1.6	5.3×3.1

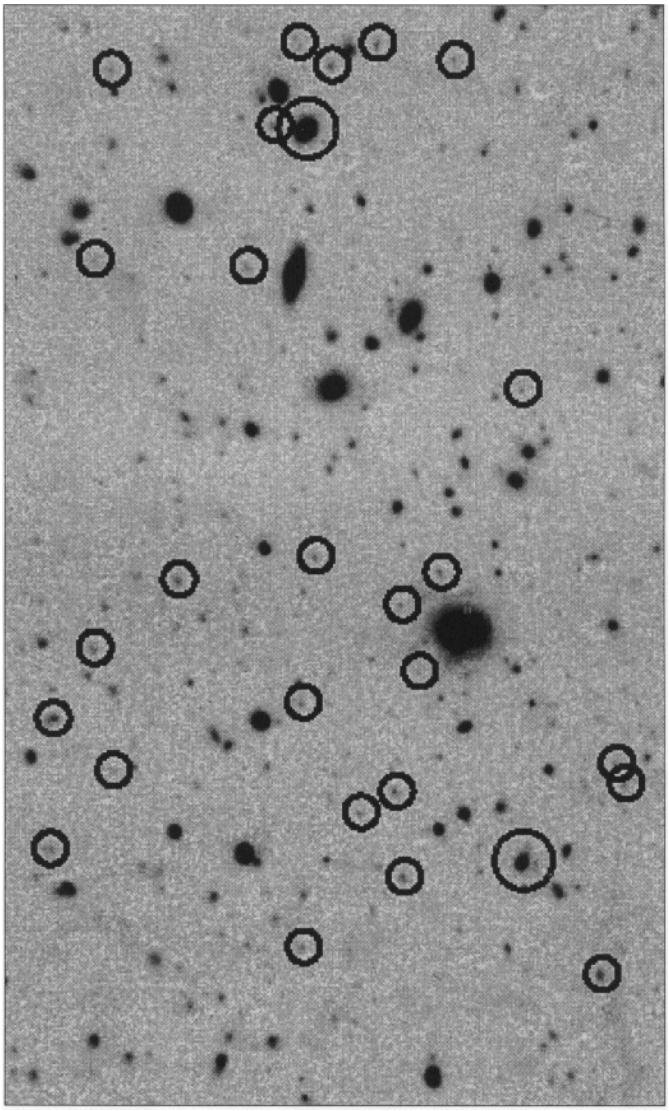

Fig. 1. Example reduced CCD frame. The R-band data frame is shown for the right ascension $12^h\,29.5^m$, declination $+26^o\,26'$ (epoch 1950.0) field of Table 1. The candidate L^* (large circles) and faint blue galaxies (small circles) from the samples of Sect. 5.1 are indicated

data, it is necessary to correct for this vignetting at the outset of data reduction. For the 1991 observations the vignetting pattern was modelled by measuring the sky background at a set of points on a rectangular grid, performing two-dimensional bicubic spline interpolation between the sampling points. A relatively coarse grid was chosen, 5 by 7 sampling points in extent, in order to lessen the possibility of removing any extended astronomical structures. The frames were then corrected for vignetting by division by the model. For the 1993 data a median filtering technique using a 45 arcsec wide filter box was employed. Flatfielding was accomplished for the 1991 data using a superflat constructed from over 100 long exposures of the night sky. For the less extensive 1993 observations the superflats were generated by coadding a number of twilight sky frames. The individual flatfield frames were vignetting-corrected before coaddition to produce the superflats; in this application the flatfielding process corrects only for the pixel-to-pixel efficiency variations and not for large-scale effects.

Cosmic ray detections were removed from the individual dark sky frames before alignment and coaddition. Candidate cosmic ray detections were identified as localised peaks rising higher than seven standard deviations above the sky background. The intensity profiles of the peaks were determined, with those steeper than a typical seeing disc being labelled as a genuine cosmic ray event. The pixel intensities in each of these detections were set to the median in surrounding pixels.

Finally the coadded images were cleaned by performing an additional median filter sky subtraction (with a 40 arcsec wide square box). Remaining spurious, low-intensity artifacts (due to dust particles on the instrumental optical surfaces) were removed via inverse unsharp masking (cf. Driver et al. 1994a). The photometric calibration of the data was accomplished using the results of pointed Hitchhiker observations of standard stars in February 1991 and May 1993, corrected to the date of observation using the nightly extinction coefficients from the Carlsberg Automated Meridian Transit Circle Telescope on La Palma. Magnitudes are expressed on the Cousins BVR_cI_c system (Cousins 1976; Bessell 1979), calibrated with Landolt (1983) photometric standards. The accuracy of the magnitude scale has been shown to be $0\overset{m}{.}1$ in each filter (Driver et al. 1994b). Colour indices are, however, more accurate because of the simultaneous recording of data through the two filters.

4. Image detection and photometry

Image detection was accomplished with a connected-pixel algorithm, using the IMAGES program of the RGASP galaxy photometry software package (Cawson 1983). For classification as a genuine image, a group of ten or more adjacent pixels ($\simeq$ 1 arcsec diameter) had to have R band intensities above a threshold of $1.5\sigma_p$ above the sky background (where σ_p represents the pixel-to-pixel standard deviation of the sky background). This minimum number of pixels corresponds to the expected minimum area of any reliably detected image due to the size of the seeing disc; given the image scale of 0.3 arcsec/pixel, this corresponds to the area within the half-maximum intensity isophote of a star under good seeing. The $1.5\sigma_p$ threshold was chosen to exclude a significant chance contribution of background pixels to the area of detected images (Driver 1994). A conservative estimate of the background standard deviation was taken, based on adopting the largest value from either: the measured background variation; a theoretical prediction of the noise in the background assuming Poisson statistics; or a value of 0.3% of the background level (based on the expectation of a 0.3% limiting accuracy of the flatfielding process on large scales). In practice, the Poissonian prediction of the background standard deviation was adopted for all four fields. To safeguard against spurious detections of random groups of sky background pixels, a signal-to-noise ratio test was used to reject low confidence detections. Monte-Carlo tests were performed on simulated data frames constructed using Poissonian noise distributions in order to assess the number of false detections retained after imposing different signal-to-noise ratio limits. Further simulations were carried out using twilight sky frames subjected to the same data reduction procedure as the night sky data. On the basis of these tests, a signal-to-noise ratio limit of 6.0 for the isophotal data was adopted. This value was found to give as few as one or two false detections per frame for the random noise simulations.

Once R band catalogues of images on the data frames had been compiled, magnitudes were determined using (variable) aperture photometry. In contrast to isophotal photometry, this technique should measure all the flux from a detected object when used with a large enough aperture size. Ideally the radius of the aperture should be chosen for a particular galaxy to include essentially all the signal from the galaxy, but not so large that it includes unnecessary noise from the sky background or nearby sources. Tyson (1988) noted that, as expected, isophotal magnitudes are close to the total magnitudes for bright objects, while Metcalfe et al. (1991) showed that aperture photometry using Kron radii (Kron, 1980) results in fixed aperture sizes for faint objects (effectively the Kron radius for a star). We therefore chose a variable circular aperture radius r_{ap} computed from the isophotal radius r_{iso} as,

$$r_{ap}{}^n = r_{iso}{}^n + r_{min}{}^n \quad , \tag{1}$$

where r_{min} and n are constants. r_{iso} was calculated from the number of pixels having intensities above the threshold of the RGASP detection process, being the radius of a circular region containing that number. r_{min} is set to 3 arcsec, about twice the typical seeing width (and in keeping with Metcalfe et al., 1991, and Lilly et al. 1991). The aperture radius therefore reduces to 3 arcsec for the faintest objects while approaching the isophotal radius for the brightest. The optimal value of the exponent n was selected on the basis of simulations of the measurement of images of face-on L* exponential disc galaxies; being circular and lacking bulge or nuclear components, these provide the most extended and flattest profiles among the conventional galaxy population. The values of r_{ap} for different values of n were calculated for different magnitudes and compared with the isophotal radius, the Kron radius and the radius containing 90% of the light. Using an exponent of n = 1.5, r_{ap} was found to be close to the 90% light radius over a wide range of total magnitudes, even at the faintest limits, and close to 2.5 Kron radii; we therefore chose to adopt n = 1.5 . Fig. 2 shows the dependence of the total detected magnitude within a circular aperture for different aperture radii for the case of face-on, exponential light profile, L* galaxies. The various curves in the figure represent different methods for defining the aperture radius.

A local measurement of the sky background surface brightness was used to remove the sky background contribution from the total signal within the aperture for each image. This was defined as the median of the pixel intensities in a 15-pixel wide circular annulus centred on the image, having an inner radius of $2.0\,r_{ap}$, excluding pixels which themselves lay within the inner radius of the equivalent annuli used to determine the background level around other images. In this way, an estimate of the background level was obtained which was essentially free of the contributions of detected images.

To avoid problems associated with incomplete data at the edges of the frames, only object images whose centres lie further than 30 pixels from the edges are considered. Fuller details of the image detection and photometric techniques are presented by Driver (1994).

The determination of the observed properties of galaxies is complicated by the overlapping of images through chance alignments. The reliable decoupling of blended images is a difficult process, complicated by factors such as the uncertainty in deciding how to assign the signal in the merged regions between the images, and the dependence of the efficiency of the process on the brightness of the image. For this analysis, if the isophotes of the two objects overlapped we simply considered the system as merged and counted it as a single image. The effects of the overlapping of images in detecting and parameterising faint galaxies in the vicinity of brighter ones are discussed in Sect. 5.3, where it is shown that overlapping images do not significantly affect the clustering statistics of interest here.

Once these principles had been used to provide R-band magnitudes for each detected image, B magnitudes were computed using the same (R band) image catalogue and the R band apertures. This method ensures that each image is treated identically in each of the two wavebands in an effort to minimise photometric errors in the colour index.

The photometric results for all four fields are displayed as a colour–magnitude diagram in Fig. 3, showing all images, both

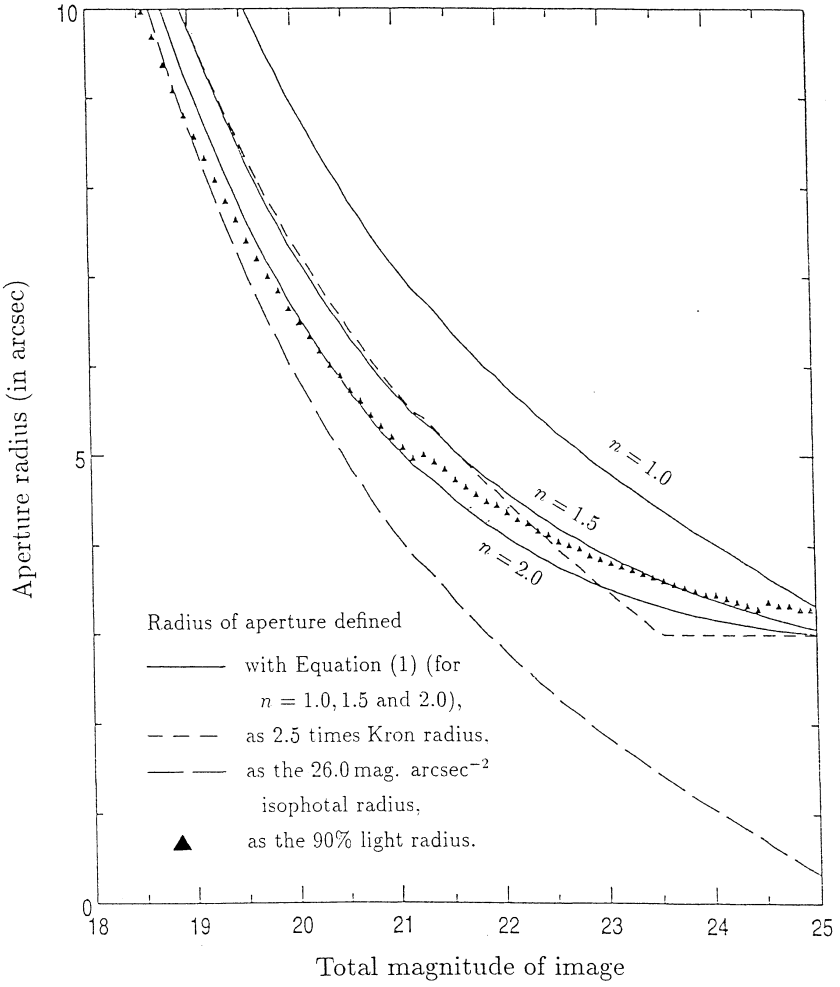

Fig. 2. A comparison of radii of variously defined photometric apertures as a function of total galaxy magnitude. The curves represent the sizes of circular apertures defined in six different ways for simulated face-on L* exponential disc galaxies. The locus for radii chosen to contain 90% of the light is shown, as is that corresponding to detection at the 26.0 mag. (arcsec)$^{-2}$ isophote. Radii set at 2.5 times the Kron (1980) radius are presented. The results of Eq. (1) are given for indices n = 1.0, 1.5 and 2.0. An index n = 1.5 was selected for the photometry of Sect. 4

stars and galaxies. The broad distribution is similar to that found by other authors (e.g. Tyson, 1988, and Metcalfe et al., 1991). The faint blue excess, however, is encountered about one magnitude brighter at any given $(B–R)_C$ colour than in many other studies. This effect is found to be pronounced among the 1993 field data, but not those from 1991. That this is not a calibration problem affecting the 1993 data is confirmed by an inspection of the $(B–R)_C$ against $(V–I)_C$ colour–colour diagram for brighter ($R < 21\overset{m}{.}0$) images; a majority of the images, which at these magnitudes are expected to contain a significant fraction of stars (50–60%), conform closely (within ± 0.15 mag) to standard (Bessell 1979, and Bell & Gustafsson 1979, 1989) stellar loci. The problem therefore affects only fainter images – if indeed it is a problem rather than some statistical fluke. While it is expected that random photometric errors will be greater for the 1993 observations due to their shorter integration times, the origin of the difference remains unclear. However, for the purposes of the present study, where colours and magnitudes need to be measured only sufficiently accurately to enable a broad classification, the excess blue tail to the colour distribution at faint magnitudes is unimportant.

5. The clustering of faint blue galaxies around L* galaxies

It should be possible to test the hypothesis that the faint blue galaxies are in reality dwarfs associated with giant galaxies if a sample of candidate giants can be identified on the basis of their observed photometric properties. We can then test the clustering of the blue galaxies around them. Magnitude-limited samples tend to select galaxies having luminosities close to L* for galaxies with properties comparable with the local population (e.g. Schechter 1976). Even for their dwarf-rich model of galaxy populations, Driver et al. (1994a) have shown that magnitude-limited samples of galaxies are likely to be dominated by giants (with intrinsic luminosities close to L* of the Schechter luminosity function) for $B < 22^m$; only at fainter magnitudes do they predict that dwarfs become increasingly important. A more conservative field galaxy luminosity function, without a sharp turn-up in the numbers of dwarfs, would predict giant domination to even fainter magnitudes. That galaxies in the $B = 20^m$ to 22^m magnitude range are dominated by L* objects is confirmed from the results of redshifts surveys (e.g. Broadhurst et al. 1988). Expecting samples of galaxies brighter than (at least) $B = 22^m$ to be rich in giant galaxies, we select candidate L* galaxies on the basis of magnitude and colour.

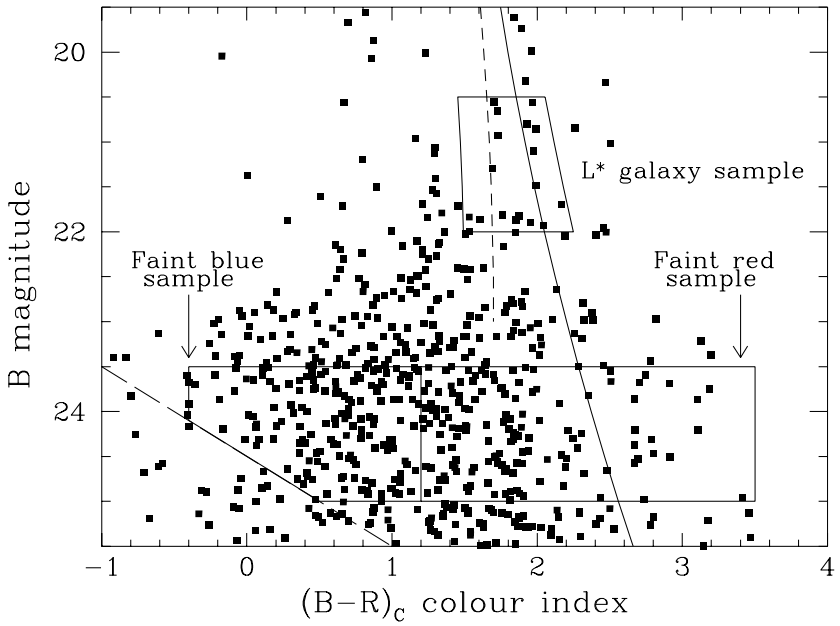

Fig. 3. The $(B–R)_c$ – B colour–magnitude diagram for the detected images of all fields, showing the candidate L*, the faint blue and the faint red galaxy samples. The solid curve is the locus corresponding to the no-evolution model of Sa-type giants. The dotted curve is the Sa giant locus displaced by an amount corresponding to Bruzual's (1983) $\mu = 0.5$ models. The dashed line illustrates the predicted completeness limit for the deepest field; all galaxies beyond this limit are rejected from the samples

A simple measure of the clustering of a sample of objects about a central point is the excess over random statistics of the objects within a particular distance of the centre (e.g. Yee & Green 1987; Longair & Seldner 1979; Aragón-Salamanca et al. 1993). Such a method is consistent with the use of the two-point angular correlation function (Phillipps & Shanks 1987a,b). Note that here we are not concerned about detecting an average excess over some overall random background; rather we are interested in the distribution of one specific set of galaxies about another specific set. We therefore do not need to consider the intricacies of data–data, data–random or random–random pairs (e.g. Landy & Szalay 1993), but simply calculate the numbers of faint blue galaxies in concentric annuli of constant thickness centred on the candidate L* objects and compare these with the corresponding results for randomly distributed points.

5.1. Selecting samples of galaxies

We choose to select a sample of candidate L* galaxies using a B magnitude range of 1.5 mag. extending to the $B = 22\overset{m}{.}0$ approximate limit of giant domination of the observed galaxy population. We further constrain the sample by imposing limits in $(B-R)_c$. The no-evolution model of galaxy colours used in Driver et al. (1994a) provides the mean $(B-R)_c$ as a function of B magnitude for Sa giants (cf. Coleman et al. 1980). We set a red limit for the candidate L* sample at $0\overset{m}{.}2$ redder than this locus to allow for photometric errors and to take some account of a distribution of galaxy properties, e.g. from E to Sc. If present, evolutionary effects would produce galaxies bluer than these colours. We define a locus in the $(B-R)_c$ – B plane accounting for evolution of the stellar populations by introducing the blueing effects of Bruzual's (1983) $\mu = 0.5$ models of spiral bulges and elliptical galaxies on the Driver et al. Sa giant model. A blue limit $0\overset{m}{.}2$ bluer than this evolution model is used for the candidate L* selection. The resultant sample contained 17 photometrically-selected images. For an $\Omega_0 = 1, \lambda_0 = 0$ cosmological model, these L* galaxies are expected to lie at redshifts of $z \simeq 0.2$ to 0.4 (cf. Koo & Kron 1992). Throughout this paper a Hubble Constant of $H_0 = 50\,\mathrm{kms}^{-1}\,\mathrm{Mpc}^{-1}$ is used.

Star–galaxy classification was attempted in order to reject star images from the sample of candidate L^* galaxies. Stars are likely to form a significant fraction of objects having the magnitudes of the L^* candidate sample and the images are sufficiently bright that image classification can be attempted. Following Jones et al. (1991), we used plots of the image central intensity against R magnitude, and of the area above the detection isophotal threshold against R magnitude for each data frame. Stellar loci were identified for each plot. The images of interest were classified according to their displacement from the appropriate stellar locus. The images were labelled as being stars, galaxies or having uncertain classifications, the process being performed independently for the central intensity and image area graphs. An overall classification was achieved through a comparison of the results of the intensity and area methods, and by visual inspection to reject merged or confused images. An object was regarded as a suitable L* galaxy if it appeared visually to be a single image and if it had received a galaxy classification under the automated tests, either through two unambiguous galaxy classifications or one galaxy and one uncertain result. Of the 17 objects in the original sample, 13 passed the star/galaxy tests. These 13 images formed the sample of candidate L* galaxies for the present study.

The sample of faint blue galaxies was selected using an apparent magnitude range of $B = 23\overset{m}{.}5$ to $25\overset{m}{.}0$; these limits are $3\overset{m}{.}0$ fainter than the equivalent ones for the candidate L* objects. The adopted colour limits were $(B-R)_c = -0\overset{m}{.}4$ to $+1\overset{m}{.}2$. An additional criterion was imposed that the galaxies

(of all four fields) lay within the predicted selection limit of the 1991 February 15 field (see Table 1); it is to be expected that photometric results outside this limit are unreliable due to the low signals involved. This limit is shown in the colour–magnitude diagram in Fig. 3.

No star/galaxy classification was attempted for the faint blue sample; at these faint magnitudes and blue colours the sample of images is dominated by galaxies, as is evident from a comparison of the star count predictions of Bahcall & Soneira (1980) with standard galaxy number counts. Indeed, at these faint magnitudes it becomes very difficult to distinguish galaxies from stars given the small image sizes compared with the seeing discs. To illustrate this point more fully, the numbers of stars expected in the faint blue galaxy samples in the four fields were computed by modelling star number counts. Using a program written and provided by Dr. G. Gilmore (briefly discussed in Gilmore 1984), star densities were computed across the (B–V) – V colour–magnitude diagram for each field by integrating the stellar populations along the sight. The three-component Gilmore–Reid–Wyse model of the Galaxy was adopted (Gilmore et al. 1989; Gilmore et al. 1990). Converting to the $(B-R)_c$ – B colour–magnitude diagram and integrating the predicted star densities over magnitude and colour provides estimates of the numbers of stars in the faint blue galaxy samples in each of the four fields. In all cases these are small, between 1 and 4 stars, as a result of the colour index limits of the sample being bluer than the majority of the main sequence stars of the (old) Galactic halo and thick disc. Due to incompleteness of the samples and to photometric errors, it is expected that the numbers of stars *observed* in the faint blue sample in each field will be smaller than the estimated numbers of stars present. We therefore choose to express the star contamination as a fraction of the total number of images present, taking the total numbers of images from the deep observations of Metcalfe et al. (1995) which are complete in all the regions of the $(B-R)_c$ – B colour–magnitude diagram of the photometrically selected samples used here. We predict a star contamination of the faint blue galaxy samples of between 1.0 % and 2.7 % in the four fields; these results are presented in full in Table 5. The presence of such small numbers of stars will not significantly affect conclusions about the clustering of the faint blue galaxies.

The faint blue galaxy sample contains 152 objects over all four fields. Because of the different K-corrections, the magnitude limits of the L^* and blue galaxy samples are displaced typically by $3\overset{m}{.}6$ in absolute B magnitude. The luminosities of the faint blue galaxies, if at the same distances as the L^* objects, would be in the range $L_B = 0.01L_*$ to $0.1L_*$, typically $L_B = 0.04L_*$. Fig. 3 shows the sample regions in the colour–magnitude diagram. Although the adopted selection criteria should produce a well-defined sample of blue galaxies, incompleteness in the R band catalogue for the less deep fields may bias the samples against the most extreme blue galaxies, possibly reducing the sensitivity of the results to the most extreme colour changes induced by galaxy interactions.

5.2. The statistics of the separations between the blue and L^* galaxies

The separations between each of the candidate L^* and blue galaxies were computed for the four fields from their R band centroid coordinates. The R band observations tend to be deeper than the B band data on account of the greater efficiency of the Hitchhiker camera at red wavelengths than blue; the R band positional data were therefore used in preference to the B band. A total of 525 separations were obtained. Fig. 4 presents a histogram of the separations between the faint blue and candidate L^* galaxies summed over all four data frames. The deviation of the observed separation distribution from an ideal linear relation is due to the finite area of the data frames. An assessment of any excess density of blue galaxies around L^* objects demands that the histogram of separations for random distributions of galaxies is known.

Monte Carlo simulations were used to model randomly distributed faint blue galaxies across the four data frames. This approach enables the effect of the finite areas of the data frames to be accounted for in detail. In order to overcome the statistical errors associated with small samples, 100 000 faint galaxies were distributed across each frame and the separations between these and the 13 observed L^* galaxies were computed. The distributions of separations for each of the four frames were normalised and added according to the number of separations from the observational data for each frame. The resultant distribution may be compared directly with the equivalent observational results; both histograms are shown in Fig. 4.

To investigate whether there is an overdensity of faint blue galaxies in the vicinity of L^* candidates, the number of separations between the two samples observed in the 10 to 60 arcsec range relative to the total number of separations were compared with the Monte Carlo simulations. The results are presented in Table 2. The observed results are clearly consistent with no observed overdensity of blue galaxies around L^* candidates on scales smaller than 1 arcmin compared with the entire 0–5 arcmin range.

5.3. The detection of faint images in the vicinity of brighter galaxies

A potential problem which complicates the interpretation of the results of Table 2 is that of a failure to detect faint galaxy images in the close vicinity of brighter galaxies (cf. Turner et al. 1993). At small separations galaxy images might become merged at the limiting detection isophote and the pixels of the fainter image might be included with those of the brighter object during the compilation of the image catalogue. A selective loss of faint galaxy images at small separations could conceal the presence of a genuine excess of faint blue galaxies around the candidate L^* objects.

The 13 galaxies of the L^* sample have image areas above the detection threshold corresponding to mean radii in the range 2.8 to 5.3 arcsec. The images of the 152 blue galaxies have mean total radii typically in the range 0.7 to 1.7 arcsec. It is there-

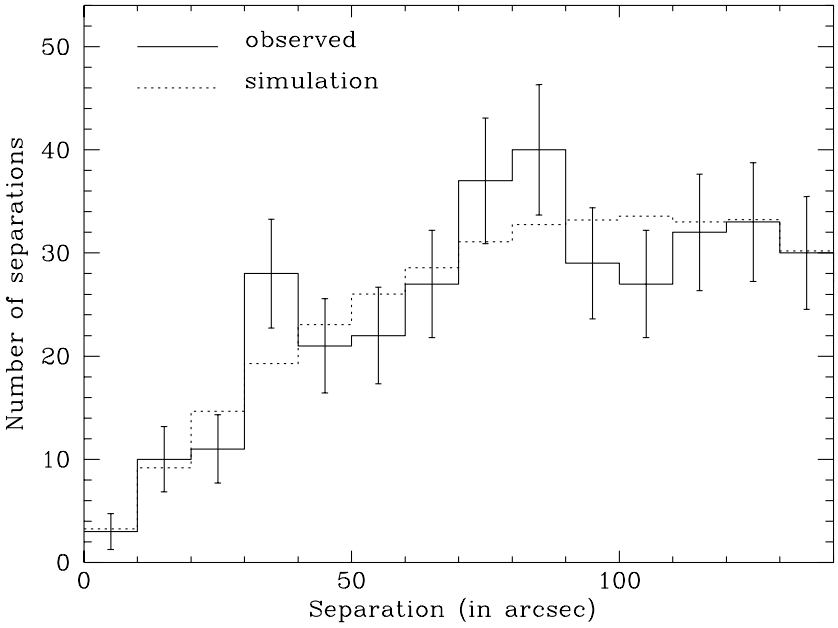

Fig. 4. The distribution of galaxy–galaxy separations between the candidate L* and faint blue galaxies. Observational results are shown using a solid line. The dotted line represents randomly distributed simulated faint blue galaxies, normalised to the scale of the observational results

Table 2. Observational results for the association of faint blue galaxies with candidate L* galaxies

Separation range (in arcsec)	Observed number of galaxy – galaxy separations	Predicted number of separations for random distributions of blue galaxies
all	525	525.00[a]
10–60	92 ± 10	92.26
15–60	88 ± 9	88.40

[a] Set by the normalisation to the number of observational results

fore to be expected that galaxy–galaxy separations of 10 arcsec and greater will not be significantly affected by the merging of images. At a typical redshift of $z = 0.3$ an apparent angular separation of 10 arcsec corresponds to a transverse physical separation of 55 kpc (for $H_0 = 50\,\mathrm{kms}^{-1}\mathrm{Mpc}^{-1}$, $q_0 = 0.5$ and zero cosmological constant).

To test this in greater detail, simulations were performed of the detection of faint images in the vicinity of example candidate L* images. The May 1993 R band data frame was selected for the study, being the least deep of the available R band observations. The frame has 4 candidate L* galaxies from the sample of Sect. 5.1. They have magnitudes in the range $R = 18\overset{\mathrm{m}}{.}8$ to $20\overset{\mathrm{m}}{.}3$. Faint blue galaxies were represented by circularly-symmetric gaussian light profiles having full-widths at half-maximum intensity equal to the measured seeing. The central intensities were selected to give a total magnitude of $R = 23\overset{\mathrm{m}}{.}5$, typical of the faint blue sample. The blue galaxies were added to the observed R band data frame, one at a time, and the image detection process of Sect. 4 applied to the frame. The image catalogue was inspected to determine whether the artificial blue galaxy had been detected as a distinct image, whether it was merged with the L* galaxy, or whether it was merged with another nearby galaxy. Faint blue galaxies were placed at distances of 5.0, 7.5, 10.0, 12.5 and 15.0 arcsec from the centroid of the L* candidate, at each of 8 positions for each separation. A total of 160 simulated images were used.

Table 3 presents the results of the simulations. While merging of the artificial faint galaxy with the L* candidate is a major problem for separations smaller than 10 arcsec, it does not significantly affect separations greater than 10 arcsec. The results of Table 2 for the interval 10 to 60 arcsec are therefore unaffected by image blending and our null result remains. Table 3 does show that merging of the blue galaxy with a third image does occur. It has been assumed that the distribution of this general background of galaxies with which some of the faint blue galaxy images merge is uniform across the frame, and therefore affects clustering statistics equally on all scales.

6. The associations between other samples of galaxies

The study of any possible association between faint blue and L* galaxies has been extended to a consideration of other samples of galaxies. A colour index test was applied to the brighter galaxies in order to select the L* candidates. It is of interest to investigate whether a relaxation of the selection criteria to include brighter galaxies of all colours affects the conclusions. Equally, any possible clustering between the brighter ($20\overset{\mathrm{m}}{.}5 \leq \mathrm{B} \leq 22\overset{\mathrm{m}}{.}0$) galaxies and all faint ($23\overset{\mathrm{m}}{.}5 \leq \mathrm{B} \leq 25\overset{\mathrm{m}}{.}0$) galaxies, the faint blue

Table 3. Statistics for the detection of faint galaxy images in the vicinity of four candidate L* galaxies

Separation between faint galaxy and L* candidate (arcsec)	Number of simulations considered	Number of times faint and L* galaxies merged	Number of times faint galaxy was a distinct image	Number of times faint galaxy was merged with a third image
5.0	32	32	0	0
7.5	32	30	2	0
10.0	32	5	18	9
12.5	32	0	20	12
15.0	32	0	22	10

with faint red galaxies, and between the faint blue galaxies and themselves have been investigated.

The selection criteria for the samples of galaxies are summarised in Table 4. The brighter images were subjected to a star/galaxy classification as described in Sect. 5.1 for the L* candidates. This reduced the number of images from 38 to 21. As in the case of the faint blue galaxies, no classification was attempted for the faint and faint red samples. Unlike the case of the faint blue samples, however, the samples will include modest numbers of main sequence stars of the Galactic halo and thick disc. Following the method of Sect. 5.1, star number densities were predicted for each galaxy sample of each of the four fields and image number densities were taken from Metcalfe et al. (1995). The resulting fractional star contaminations are presented in Table 5. The effect of stars is in general small, although the fourth field, lying at intermediate galactic latitude, does experience some significant contamination to the red galaxies sample.

Galaxy–galaxy separations were calculated between the members of different samples, as presented in Table 6. The table lists the total number of galaxy–galaxy separations and the number of separations in the range 10 to 60 arcsec.

Detailed Monte-Carlo simulations were performed for each pair of samples to predict the number of separations in the 10 to 60 arcsec range, using large numbers of random points to reduce numerical noise, normalising the results to the observed total number of separations in each frame. The bright–faint blue galaxies simulation used the observed bright galaxy data, but 100 000 simulated random faint blue images for each frame. Two simulations were performed for the faint blue–faint red samples: one (case (a) in Table 6) used 20 000 random blue galaxies and the observed red on each frame; the other (case (b)) used the observed blue and 20 000 random red galaxies on each frame. The bright–faint galaxy study again used the observed bright galaxy data, with 100 000 simulated random faint images on each frame. The simulation of the association of faint blue galaxies with themselves was firstly (case (a)) performed using the observed blue galaxies and 20 000 random points on each data frame, then again (case (b)) with a single random sample of 2000 galaxies per frame computing the separations internal to the random sample. All simulation results were normalised to the observed total number of separations.

7. An investigation of the errors in the results

To assess whether there exists any observed excess or deficiency in the number of galaxies of one type in the vicinity of galaxies of another, it is necessary to understand the error in the number of galaxy–galaxy separations in the 10 to 60 arcsec range. A naïve estimate of the error in the number of separations might be as the square root of the number. However, individual separation results will be highly correlated and such a simplistic approach may provide an incorrect error estimate, leading to inappropriate statistical conclusions.

Detailed numerical simulations have been performed of the statistics of galaxy distributions. Randomly distributed galaxies were placed in four simulated data frames corresponding to the samples of Table 4, having the numbers of the observed data. The galaxy–galaxy separations were determined and the number in the 10 to 60 arcsec range calculated. This process was performed repeatedly a total of 200 times for each pair of galaxy samples. The statistics of the number of separations in the 10 to 60 arcsec range provided estimates of the errors in the individual results of Tables 2 and 6; these are the errors quoted in these tables.

The Monte Carlo estimates of the error are larger than a simplistic $\sqrt{n}$ estimate, particularly for the bright–faint, the faint blue–faint red, and especially the faint blue–faint blue cases. Indeed had the naïve estimate been used, it would have given a false anticorrelation between faint blue galaxies at a 2.6-sigma confidence level.

The results obtained using the detailed error assessments are presented in Table 7.

8. Discussion

The results presented in Table 7 show no statistically significant evidence of any preferential clustering of galaxies of one type about those of another for any of the pairs of samples investigated. In particular, there is no evidence of any association of the faint blue galaxies about candidate luminous galaxies.

The candidate L*–faint blue galaxy study found 92 ± 10 galaxy–galaxy separations in the 10 to 60 arcsec range, using 13 L* candidates. The predicted number for a random distribution of blue galaxies was 92.26 . This gives an excess number of separations of -0.26 ± 10 in this range, equivalent to an overdensity of -0.02 ± 0.76 blue galaxies per L* candidate.

Table 4. Selection criteria for samples of galaxies. The selection criteria for the samples of galaxies are summarised in the table. An additional constraint was imposed that the image lay within the expected selection limits of the 1995 February 15 data. In practice this affected the most extreme faint blue galaxies only

Galaxy sample	Magnitude limits	Colour index limits	Star/galaxy test	Visual test	Number in sample
L* candidates	$20\overset{m}{.}5 \leq B \leq 22\overset{m}{.}0$	See Sect. 5.1	Yes	Yes	13
Faint blue	$23\overset{m}{.}5 \leq B \leq 25\overset{m}{.}0$	$-0\overset{m}{.}4 \leq (B–R)_C \leq +1\overset{m}{.}2$	No	No	152
Bright	$20\overset{m}{.}5 \leq B \leq 22\overset{m}{.}0$	$-0\overset{m}{.}5 \leq (B–R)_C \leq +3\overset{m}{.}5$	Yes	Yes	21
Faint red	$23\overset{m}{.}5 \leq B \leq 25\overset{m}{.}0$	$+1\overset{m}{.}2 \leq (B–R)_C \leq +3\overset{m}{.}5$	No	No	138
All faint	$23\overset{m}{.}5 \leq B \leq 25\overset{m}{.}0$	$-0\overset{m}{.}5 \leq (B–R)_C \leq +3\overset{m}{.}5$	No	No	304

Table 5. Star contamination of the galaxy samples

Field		Galactic coordinates		Estimated fractional star contamination		
R.A.	Dec.	Long.	Lat.	Faint blue sample	Faint red sample	All faint sample
$12^h\,29\overset{m}{.}5$	$+26^\circ\,26'$	224°	$+86^\circ$	1.0 %	9.4 %	3.5 %
11 40.1	+19 49	235	+73	1.0 %	8.6 %	3.2 %
13 37.8	+11 28	341	+70	1.7 %	18 %	6.4 %
15 47.6	+21 35	35	+49	2.7 %	37 %	13 %

L* galaxies having B = $20\overset{m}{.}5$ to $22\overset{m}{.}0$ would lie at redshifts of z = 0.23 to 0.36, adopting $M_B^* = -21\overset{m}{.}0$, K-corrections appropriate to Sab galaxies (Driver et al. 1994), H_0 = 50 kms^{-1}Mpc^{-1}, q_0 = 0.5 and zero cosmological constant. At a typical redshift of z = 0.30, a 60 arcsec angular radius about the L* galaxy corresponds to a physical radius of 330 kpc (the expected limit for potential merging victims, as discussed in Sect. 2). Thus a 2.5 sigma upper limit of 1.9 blue galaxies within this region corresponds to a projected mean excess density of 5.6 Mpc^{-2}.

It is informative to compare this limit with the predicted number of dwarf galaxies of all colours within the 330 kpc radius, having similar magnitudes to the blue galaxies, which would be given by the local galaxy population extrapolated to z = 0.30. The B = $23\overset{m}{.}5$ to $25\overset{m}{.}0$ apparent magnitude limits for the faint blue galaxy sample corresponds to $M_B = -18\overset{m}{.}3$ to $-16\overset{m}{.}8$ at z = 0.30 for K-corrections typical of dwarf irregulars, or $-19\overset{m}{.}2$ to $-17\overset{m}{.}7$ if they are dwarf ellipticals. In either case, using the Efstathiou et al. (1988) local parameterisation of the Schechter luminosity function (with a faint end slope $\alpha = -1.07$), the number density of conventional (having the properties of the local population) dwarf galaxies of all colours passing the apparent magnitude selection test of the faint blue galaxies is predicted to be $\simeq$ 0.008Mpc^{-3} in the absence of evolution after applying a $(1+z)^3$ volume scaling. A steeper faint end of the galaxy luminosity function, with $\alpha = -1.25$, would increase this by a factor of $\simeq 2$, as would a rescaling of the luminosity function to fit the galaxy counts at $B \simeq 18$ (see e.g. Metcalfe et al. 1995; Glazebrook et al. 1995c).

From Phillipps (1985a,b) and Phillipps & Shanks (1987a) we see that the expected projected excess number density of galaxies within an angular radius corresponding to a projected physical separation s from a galaxy is related to the amplitude of the correlation function r_0 by

$$E(<s) \;=\; \frac{2}{3-\gamma}\, G(\gamma)\, r_0^{\gamma}\, s^{1-\gamma}\, \phi_{int} \quad ,$$

where γ is the index of the spatial two-point correlation function $\xi(r) = (r/r_0)^{-\gamma}$, $G(\gamma)$ is a constant (= 3.6791 for γ = 1.8), and ϕ_{int} is the integral of the galaxy luminosity function between the two absolute magnitude limits of the sample. Assuming a number density of faint blue galaxies equal to that of a conventional (local, no evolution, with only density scaling) galaxy population at $z \simeq 0.3$, the 2.5σ upper limit on the clustering amplitude is then $r_0 < 9$ Mpc for a standard flat luminosity function or $r_0 < 5$ Mpc for a slightly steeper one or one with a higher normalisation. If the faint blue galaxies actually have a higher space density (e.g. Phillipps & Driver 1995; Driver et al., 1995b), then their clustering amplitude drops correspondingly. In any of these cases there is certainly no evidence for strong clustering of the faint blue galaxies about L^* primaries: the numbers observed are consistent with (or more likely less than) the numbers expected for galaxies with 'average' clustering ($r_0 \simeq 10$ Mpc; see e.g. Peebles 1980). The 1σ limit $0 < r_0 \lesssim 4$ Mpc for the cross-correlation would be consistent with the low clustering amplitude seen for the faint blue galaxies themselves (see e.g. Efstathiou et al. 1991; Roukema & Peterson 1994). In particular, Brainerd et al. (1995) find that their data at R $\sim$ 24 (B $\sim$ 25) are consistent with $r_0 \simeq 2.0$ Mpc. Similar results are implied by the work of Couch, Jurcevic & Boyle (1993) and Roche et al. (1993). Brainerd et al. conclude that the clustering evolution that would be needed if the faint blue galaxies (or rather, their present day descendents) had the same correlation function as 'normal' giants is physically implausible, and prefer to identify them with a weakly clustered component (perhaps dwarf irregulars, see e.g., Thuan et al. 1991, Santiago & da Costa 1990).

Table 6. Galaxy–galaxy separation results for additional samples of galaxies. The numbers of galaxy–galaxy separations between the various samples are presented for the observational data for both the entire range of separations and for the restricted range 10" to 60". Error estimates are taken from Sect. 7. For comparison the results of the Monte Carlo simulations for randomly distributed points are presented in columns 5 and 6 for the same separation ranges. For the faint blue–faint red study, simulated case (a) refers to random blue and the observed red galaxies; case (b) refers to the observed blue and simulated red galaxies. In the faint blue–faint blue study, case (a) represents the statistics for one observed and one random blue sample, while case (b) refers to the intercorrelations of a single random sample

First sample	Second sample	Number of observed separations		Normalised number from simulations	
		Total	10" to 60"	Total range	10" to 60"
Bright	Faint blue	860	146 ± 15	860.0	144.95
Faint blue	Faint red	4753	847 ± 36	4753.0	887.02 (a)
					851.12 (b)
Bright	All faint	1586	289 ± 24	1586.0	279.25
Faint blue	Faint blue	6178	994 ± 59	6178.0	1087.83 (a)
					1076.72 (b)

Table 7. Statistical conclusions. The excess densities over random distributions of galaxies are presented for each pair of samples considered. Simulation sets (a) and (b) are as in Table 6 for the faint blue–faint red and faint blue–faint blue studies

First sample	Second sample	Observed overdensity	Overdensity / error
Candidate L$*$	Faint blue	0.0 ± 10	-0.0
Bright	Faint blue	$+1 \pm 15$	+0.1
Faint blue	Faint red	-40 ± 36 (a)	-1.1
		-4 ± 36 (b)	-0.1
Bright	All faint	$+10 \pm 24$	+0.4
Faint blue	Faint blue	-94 ± 59 (a)	-1.5
		-83 ± 59 (b)	-1.4

This is certainly consistent with our finding of very weak clustering of the faint blue population about giants, too (for redshifts around 0.2 to 0.4). Using HST data, Burkey et al. (1994) have found relatively few close companions around field galaxies at $z \simeq 0.5$ to 0.7 . Recently, Le Fèvre et al. (1996) have used redshift data to show that magnitude $17\overset{\mathrm{m}}{.}5 \leq \mathrm{I}_{AB} \leq 22\overset{\mathrm{m}}{.}5$ galaxies at redshifts $0.2 \leq z \leq 0.5$ exhibit weak spatial clustering, consistent with these results.

The study of the clustering between the other samples of galaxies reveals no evidence of correlations within the estimated errors. It should be noted that the contamination of the samples of faint galaxies by stars (estimated in Table 5) should not affect the results of Table 7. The presence of a *random* population of images in any galaxy sample will not affect the overdensity in excess of a random distribution found within 60 arcsec of other galaxy. The only effect of star contamination will be to increase the errors present in the overdensities; as the total number of images in the samples – including stars – have been used in the error calculations of Sect. 7 and Table 6, these results are unaffected.

Studies of the angular two-point correlation function of galaxies at faint magnitudes find an amplitude smaller than that for brighter magnitudes (e.g. Efstathiou et al. 1991; Neuschaefer et al. 1991; Roche et al. 1993). Adopting an amplitude of the correlation function of $w \simeq 0.02$ at an angular separation of 30" for $\mathrm{B} \simeq 23\overset{\mathrm{m}}{.}5$ to $25\overset{\mathrm{m}}{.}0$ galaxies (see the review of Efstathiou 1995), and an angular dependence of $w(\theta) \propto \theta^{\,0.8}$, predicts an excess of 1.7% faint galaxies about other faint galaxies in the 10" to 60" separation range. This compares with the observed *under*density of (7.7 ± 5.5) % for the faint blue galaxies of the current study.

9. Conclusions

No evidence is found, within the errors in the data, for an association between the faint blue galaxies and L* candidates for separations less than 1 arcmin, corresponding to scales of $\lesssim$ few hundred kpc. This is inconsistent with some merger models of galaxy evolution which predict that the faint blue galaxies have nearby parent giants with which they later merge; if this effect did occur significantly, it would have to be at a redshift > 0.4 . Similarly, although a complete understanding of galaxy mergers is still lacking, recent work on the hierarchical merging of haloes (e.g. Kauffmann & White 1993; Lacey & Cole 1993; Kauffmann et al. 1994; Cole et al. 1994) may suggest that, while giant galaxies could well be built up in this way, the merger rate may not be sufficient to explain the very large numbers of faint galaxies actually seen (pre-merger sub-units in this theory). Our current result may therefore be additional evidence in favour of a fading scenario over merging as being the fate of the faint blue galaxy population, at least to the extent that the latter are seen at moderate redshifts, as is usually presumed.

Acknowledgements. The authors would like to acknowledge the contribution of the other Hitchhiker team members, in particular Craig McKay, Nick Rees, Hugh Lang and Rhys Morris. Richard Ellis is thanked for constructive comments relating to data reduction, image

detection and faint galaxies. We also thank Rogier Windhorst for discussions on faint galaxy clustering and the HST results. Gerry Gilmore is thanked for providing his Galactic star number counts modelling program. Some data reduction and analysis was performed using computing equipment and software provided by the Starlink project. The William Herschel Telescope is operated on the island of La Palma by the Royal Greenwich Observatory in the Spanish Observatorio del Roque de los Muchachos of the Instituto de Astrofisica de Canarias. We thank the staff of the observatory for their help and cooperation. Finally we thank all the scheduled observers who allowed Hitchhiker to operate in parallel with their observations.

References

Aragón-Salamanca A., Ellis R. S., Schwartzenberg J. M., Bergeron J. A., 1993, ApJ 421, 27
Bahcall J. N., Soneira R. M., 1980, ApJS 44, 73
Bell R. A., Gustafsson B., 1978, A&AS 34, 229
Bell R. A., Gustafsson B., 1989, MNRAS 236, 653
Bernstein G. M., Tyson J. A., Brown W. R., Jarvis J. F., 1994, ApJ 426, 516
Bessell M. S., 1979, PASP 91, 589
Brainerd T. G., Smail I. R., Mould J. R., 1995, MN 275, 781
Broadhurst T. J., Ellis R. S., Glazebrook K., 1992, Nature 355, 55
Broadhurst T. J., Ellis R. S., Shanks T., 1988, MNRAS 235, 827
Bruzual G., 1983, ApJ 273, 105.
Burkey J. M., Keel W. C., Windhorst R. A., Franklin B. E., 1994, ApJ 429, L13
Carlberg R. G., 1992, ApJ 399, L31
Carlberg R. G., Charlot S., 1992, ApJ 397, 5
Casertano S., Ratnatunga K. U., Griffiths R. E., Im M., Neuschaefer L. W., Ostrander E. J., Windhorst R. A., 1995, ApJ 453, 599
Cawson M. G. M., 1983, Ph.D. thesis, University of Cambridge.
Cole S., Aragón-Salamanca A., Frenk C. S., Navarro J., Zepf S. E., 1994, MNRAS 271, 781
Cole S., Ellis R. S., Broadhurst T. J., Colless M. M., 1994, MNRAS 267, 541
Coleman G. D., Wu C.-C., Weedman D. W., 1980, ApJS 43, 393
Colless M. M., Ellis R. S., Broadhurst T. J., K. Taylor K., Peterson B. A., 1993, MNRAS 261, 19
Colless M. M., Ellis R. S., Taylor K., Hook R. N., 1990, MNRAS 244, 408
Colless M. M., Schade D., Broadhurst T. J., Ellis R. S., 1994, MNRAS 267, 1108
Couch W. J., Jurcevic J. S., Boyle B. J., 1993, MNRAS, 260, 241
Cousins A. W. J., 1976, Mem. R. Astron. Soc. 81, 25
Cowie L. L., Hu E. M., Songaila A., 1995, AJ 110, 1576
Cowie L. L., Songaila A., Hu E. M., 1991, Nat 354, 460
Dalcanton J. J., 1993, ApJ 415, L87
Driver S. P., 1994, Ph.D. thesis, University of Wales, Cardiff.
Driver S. P., Phillipps S., Davies J. I., Morgan I., Disney M. J., 1994a, MNRAS 266, 155
Driver S. P., Phillipps S., Davies J. I., Morgan I., Disney M. J., 1994b, MNRAS 268, 393
Driver S. P., Windhorst R. A., Ostrander E. J., Keel W. C., Griffiths R. E., Ratnatunga K. U., 1995a, ApJ 449, L23
Driver S. P., Windhorst R. A., Griffiths R. E.,1995b, ApJ 453, 48
Efstathiou G., 1995, MNRAS 272, L25
Efstathiou G., Bernstein G., Katz N., Tyson J. A., Guhathakurta P., 1991, ApJ 380, L47
Efstathiou G., Ellis R. S., Peterson B. A., 1988, MNRAS 232, 431
Giraud E., 1992, A&A 257, 501
Gilmore G., 1984, MNRAS 207, 223
Gilmore G., King I. R., van der Kruit, P. C., 1990, in The Milky Way as a Galaxy, University Science Books, Mill Valley, California
Gilmore G., Wyse R. F. G., Kuijken K., 1989, ARA&A 27, 555
Glazebrook K., Ellis R. S., Colless M. M., Broadhurst T. J., Allington-Smith J., Tanvir N., 1995a, MNRAS 273, 157
Glazebrook K., Ellis R. S., Santiago B., Griffiths R. E., 1995b, MNRAS 275, L19
Glazebrook K., Peacock J. A., Miller L., Collins C. A., 1995c, MNRAS 275, 169
Jones L. R., Fong R., Shanks T., Ellis R. S., Peterson B. A., 1991, MNRAS 249, 481
Jones J. B., Driver S. P., Davies J. I., Phillipps S., Morgan I., Disney M. J., 1994, In the Proceedings, I.A.U. Symposium No. 161, Astronomy from Wide-field Imaging, ed. H. T. MacGillivray, E. B. Thomson, B. M. Lasker, I. N. Reid, D. F. Malin, R. M. West & H. Lorenz, Kluwer Academic Publishers, pp. 77-78.
Kauffmann G., Guiderdoni B., White S. D. M., 1994, MNRAS 267, 981
Kauffmann G., White S. D. M., 1993, MNRAS 261, 921
Koo D. C., 1990, In the Proceedings, Edwin Hubble Centennial Symposium, Evolution of the Universe of Galaxies, ed.R. G. Kron, Astron. Soc. Pacific, San Francisco, pp. 268–285.
Koo D. C., Guzmán R., Faber S. M., Illingworth G. D., Bershady M. A., Kron R. G., Takamiya M., 1995, ApJ 440, L49
Koo D. C., Kron R. G., 1992, ARA&A 30, 613
Kron R. G., 1980, ApJS, 43, 305
Lacey C., Cole S., 1993, MNRAS 262, 627
Landolt A. U., 1983, AJ 88, 439
Landy S. D., Szalay A., 1993, ApJ 412, 64
Le Fèvre O., Hudon D., Lilly S. J., Crampton D., Hammer F., Tresse L., 1996, ApJ 461, 534
Lilly S. J., Cowie L. L., Gardner J. P., 1991, ApJ 369, 79
Longair M. S., Seldner M., 1979, MNRAS 189, 433
Metcalfe N., Shanks T., Fong R., Jones L. R., 1991, MNRAS 249, 498
Metcalfe N., Shanks T., Fong R., Roche N., 1995, MNRAS 273, 257
Neuschaefer L., Windhorst R. A., 1995, ApJ 439, 14
Neuschaefer L., Windhorst R. A., Dressler A., 1991, ApJ 382, 32
Peebles P. J. E., 1980, The Large-Scale Structure of the Universe, Princeton University Press, Princeton, New Jersey.
Phillipps S., 1985a, MNRAS 212, 657
Phillipps S., 1985b, Nature 314, 721
Phillipps S., Driver S. P., 1995, MNRAS 274, 832
Phillipps S., Shanks T., 1987a, MNRAS 227, 115
Phillipps S., Shanks T., 1987b, MNRAS 229, 621
Pritchet C. J., Infante L., 1992, ApJ 399, L35
Rocca-Volmerange B., Guiderdoni B., 1990, MNRAS 247, 166
Roche N., Shanks T., Metcalfe N., Fong R., 1993, MNRAS 263, 360
Roukema B. F., Peterson B. A., 1994, A&A 285, 361
Santiago B. X., da Costa L. N., 1990, ApJ 362, 386
Schechter P., 1976, ApJ 203, 297
Thuan T. X., Alimi J.-M., Gott J. R., Schneider S. E., 1991, ApJ 370, 25
Tóth G., Ostriker J. P., 1992, ApJ 389, 5
Turner J. A., Phillipps S., Davies J. I., Disney M. J., 1993, MNRAS 261, 39
Tyson J. A., 1988, AJ 96, 1
Woods D., Fahlman G. G., Richer H. B., 1995, ApJ 453, 583
Yee H. K. C., Green R. F., 1987, ApJ 319, 28
Zepf S. E., Koo D. C., 1989, ApJ 337, 34